

波纹倾角 β 对空气在波纹流道内的流阻 与传热影响的数值分析

吴华新¹, 孙刚¹, 周松², 田宝仁³

(1. 哈尔滨工程大学 建筑工程学院, 黑龙江 哈尔滨 150001; 2. 哈尔滨工程大学 动力工程学院, 黑龙江 哈尔滨 150001;
3. 吉泰换热器厂, 吉林 四平 136001)

摘 要: 空气—水波纹板式加热器不同于传统的肋片管式加热器, 它是一次表面换热器, 具有结构紧凑、高效的特点, 可用于气—水加热与热能回收等场合。利用 Fluent 对空气在波纹倾角 $\beta = 30^\circ, 45^\circ$ 和 60° 流道内的流阻与传热特性进行了模拟, 计算了表面摩擦系数 f 、努塞尔数 Nu 及传热因子与表面摩擦系数的比值 j/f , 表明波纹倾角是影响空气在波纹流道内的流阻与传热过程的一个重要因素, 通过比较可为进一步优化设计空气—水波纹板式加热器提供一定的参考。

关 键 词: 空气—水波纹板加热器; 流阻; 传热; 数值分析

中图分类号: TK124 文献标识码: A

引 言

目前换热设备的空气加热器通常采用肋(翅)片管的形式, 如图 1 所示, 强化空气侧传热^[1]。肋片是光管外的二次表面, 在增加传热面积来强化传热的同时也增加了传热热阻。波纹板式空气—水加热器是由波纹板片叠装而成, 采用的是不同于传统的空气加热器的设计思想, 传热介质与换热表面直接接触的一次表面, 不存在翅片效率高低的问题^[2], 具有传热系数高、压降小、结构紧凑等优点。

空气—水波纹板式加热器综合了水—水板式换热器与微型燃气轮机回热器的一次换热表面的传热过程^[3-9], 如图 2 所示。通过波纹板的叠加组合, 分别形成空气与水各自的流道, 使低温流体(空气)的两侧为高温流体(水)所包围加热; 反之, 高温流体被低温流体双面冷却。由于波纹板的反向叠合及板片上波纹的存在, 叠合后的波纹板片间形成断面形状周期性变化的复杂三维流道。倾斜的波纹对流体在流动方向上产生扰动, 形成二次流, 流体的边界层不断地被破坏, 使流体在低雷诺数下形成湍流, 强化传热。水和空气是热物性相差很大的两种流体, 强化

空气侧传热是其关键。空气在流道内的流阻与传热过程受波纹倾角 β (流体速度方向与波纹脊线方向的夹角)、波纹形状影响较大。本研究利用 Fluent 对 3 种波纹倾角 $\beta = 30^\circ, 45^\circ$ 和 60° 的相同形状的多边形波纹板进行模拟, 通过比较有助于认识空气在波纹板间的流动与传热规律, 为开发紧凑、高效的空气—水换热器提供参考。

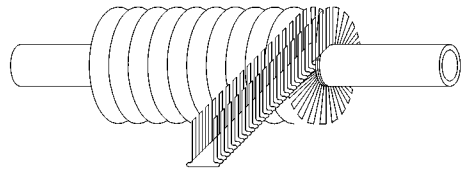


图 1 肋片管结构

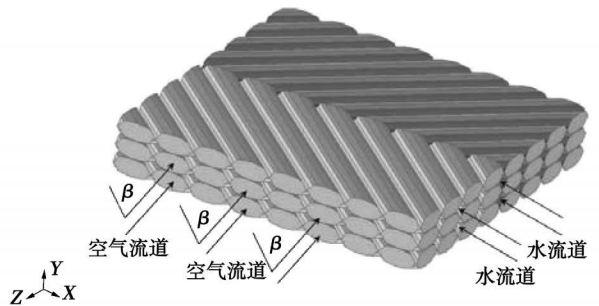


图 2 空气—水波纹板式加热器传热结构

1 计算的物理问题及模型的建立

选取具有代表性的传热区域进行模拟。本研究的 3 个计算对象区域如图 3 所示, 分别为两块长为 $128 \text{ mm} \times 128 \text{ mm}$ 的正方形波纹板叠加而成, 波纹为人字形, 波纹夹角分别取 $\beta = 30^\circ, 45^\circ$ 和 60° , 上层的波纹板与下层的波纹板反向放置, 波纹形状为多边形, 目的是扩大波纹板间空气侧的流道, 波纹的形状

尺寸如图 4 所示, 详细尺寸见表 1, 节距 $\lambda=16$ mm。

此三维模型的建立与网格划分采用 Fluent 的前处理软件 Gambit 实现, 建立如图 3 所示的物理模型。网格划分采用六面体网格, 网格大小为 0.7, 网格数约为 2×10^6 。

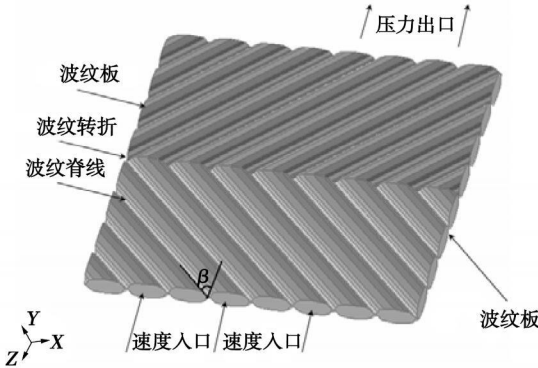


图 3 计算区域三维结构

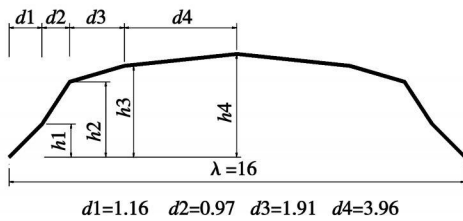


图 4 单个波纹的结构尺寸

表 1 波纹的高度尺寸 (mm)

h_1	h_2	h_3	h_4
1.16	2.63	3.19	3.60

2 控制方程的建立及其求解过程

2.1 控制方程

对所计算的物理模型作如下简化:

- (1) 稳态、常物性和不可压。
- (2) 受迫流动(忽略浮升力的影响)。
- (3) 忽略板片与流体间的辐射传热。

将简化后的物理模型建立数学模型为三维标准

$k-\epsilon$ 两方程湍流模型方程组:

$$\text{div}(\rho V \phi) = \text{div}(\Gamma \text{grad} \phi) + S$$

连续方程:

$$\frac{\partial(\rho u)}{\partial x} + \frac{\partial(\rho v)}{\partial y} + \frac{\partial(\rho w)}{\partial z} = 0$$

式中: ρ —密度, kg/m^3 ; u, v —气体的速度矢量在 x, y 和 z 方向的分量。

动量方程:

$$\frac{\partial(\rho u u)}{\partial x} + \frac{\partial(\rho u v)}{\partial y} + \frac{\partial(\rho u w)}{\partial z} = \frac{\partial}{\partial x}(\mu_{\text{eff}} \frac{\partial u}{\partial x}) + \frac{\partial}{\partial y}(\mu_{\text{eff}} \frac{\partial u}{\partial y}) + \frac{\partial}{\partial z}(\mu_{\text{eff}} \frac{\partial u}{\partial z}) - \frac{\partial p}{\partial x} + s_u$$

$$\frac{\partial(\rho v u)}{\partial x} + \frac{\partial(\rho v v)}{\partial y} + \frac{\partial(\rho v w)}{\partial z} = \frac{\partial}{\partial x}(\mu_{\text{eff}} \frac{\partial v}{\partial x}) + \frac{\partial}{\partial y}(\mu_{\text{eff}} \frac{\partial v}{\partial y}) + \frac{\partial}{\partial z}(\mu_{\text{eff}} \frac{\partial v}{\partial z}) - \frac{\partial p}{\partial y} + s_v$$

$$\frac{\partial(\rho w u)}{\partial x} + \frac{\partial(\rho w v)}{\partial y} + \frac{\partial(\rho w w)}{\partial z} = \frac{\partial}{\partial x}(\mu_{\text{eff}} \frac{\partial w}{\partial x}) + \frac{\partial}{\partial y}(\mu_{\text{eff}} \frac{\partial w}{\partial y}) + \frac{\partial}{\partial z}(\mu_{\text{eff}} \frac{\partial w}{\partial z}) - \frac{\partial p}{\partial z} + s_w$$

$$(\mu_{\text{eff}} \frac{\partial w}{\partial y}) + \frac{\partial}{\partial z}(\mu_{\text{eff}} \frac{\partial w}{\partial z}) - \frac{\partial p}{\partial x} + s_w$$

$$(\mu_{\text{eff}} \frac{\partial w}{\partial x}) + \frac{\partial}{\partial z}(\mu_{\text{eff}} \frac{\partial w}{\partial z}) - \frac{\partial p}{\partial x} + s_w$$

式中: $\mu_{\text{eff}} = \mu + \mu_t$ 湍流有效粘度, $\text{Pa} \cdot \text{s}$; μ —分子粘度, 是物性参数; μ_t —湍动粘度, $\mu_t = \rho C_\mu \frac{k^2}{\epsilon}$, 大小取决于流态; p —流体微元体上的压力, Pa ; s_u, s_v 和 s_w —动量守恒方程的广义源项。

能量守恒方程:

能量守恒方程:

$$\frac{\partial(\rho u T)}{\partial x} + \frac{\partial(\rho v T)}{\partial y} + \frac{\partial(\rho w T)}{\partial z} = \frac{\partial}{\partial x}(\frac{\lambda \partial T}{c_p \partial x}) + \frac{\partial}{\partial y}(\frac{\lambda \partial T}{c_p \partial y}) + \frac{\partial}{\partial z}(\frac{\lambda \partial T}{c_p \partial z}) + s_T$$

$$\frac{\partial T}{\partial y} + \frac{\partial}{\partial z}(\frac{\lambda \partial T}{c_p \partial z}) + s_T$$

式中: T —温度, K ; c_p —气体比热, $\text{J}/(\text{kg} \cdot \text{K})$; λ —流体的传热系数, $\text{W}/(\text{m}^2 \cdot \text{K})$; s_T —流体的粘性耗散项。

标准 $k-\epsilon$ 模型方程:

k 方程:

$$\frac{\partial(\rho k u)}{\partial x} + \frac{\partial(\rho k v)}{\partial y} + \frac{\partial(\rho k w)}{\partial z} = \frac{\partial}{\partial x}(\mu + \frac{\mu_t \partial k}{\sigma_k \partial x}) + \frac{\partial}{\partial y}(\mu + \frac{\mu_t \partial k}{\sigma_k \partial y}) + \frac{\partial}{\partial z}(\mu + \frac{\mu_t \partial k}{\sigma_k \partial z}) + \rho G_k - \rho \epsilon$$

$$(\mu + \frac{\mu_t \partial k}{\sigma_k \partial y}) + \frac{\partial}{\partial x}(\mu + \frac{\mu_t \partial k}{\sigma_k \partial x}) + \rho G_k - \rho \epsilon$$

ϵ 方程:

$$\frac{\partial(\rho \epsilon u)}{\partial x} + \frac{\partial(\rho \epsilon v)}{\partial y} + \frac{\partial(\rho \epsilon w)}{\partial z} = \frac{\partial}{\partial x}(\mu + \frac{\mu_t \partial \epsilon}{\sigma_\epsilon \partial x}) + \frac{\partial}{\partial y}(\mu + \frac{\mu_t \partial \epsilon}{\sigma_\epsilon \partial y}) + \frac{\partial}{\partial z}(\mu + \frac{\mu_t \partial \epsilon}{\sigma_\epsilon \partial z}) + \frac{c_{1\epsilon} \epsilon}{k} G_k - c_{2\epsilon} \rho \frac{\epsilon^2}{k}$$

$$\frac{\partial}{\partial x}(\mu + \frac{\mu_t \partial \epsilon}{\sigma_\epsilon \partial x}) + \frac{\partial}{\partial y}(\mu + \frac{\mu_t \partial \epsilon}{\sigma_\epsilon \partial y}) + \frac{\partial}{\partial z}(\mu + \frac{\mu_t \partial \epsilon}{\sigma_\epsilon \partial z})$$

$$+ \frac{c_{1\epsilon} \epsilon}{k} G_k - c_{2\epsilon} \rho \frac{\epsilon^2}{k}$$

式中: k —湍动能; ϵ —湍动耗散率; σ_k 和 σ_ϵ —与湍动能 k 和湍动耗散率 ϵ 对应的 Prandtl 数; $c_{1\epsilon}$ 和 $c_{2\epsilon}$ 为经验常数。在标准 $k-\epsilon$ 模型中, 根据文献[12]模型常数的取值如表 2 所示。

2.2 流动传热分析的有关参数与定义

式中: 水力直径 $d_e, d_e = 4s/c, \text{m}$; s —波纹板截面积, m^2 ; c —参与传热截面的湿周长, m ; 雷诺数 $Re = \rho u d_e / \mu$; 努塞耳数 $Nu = \alpha d_e / \lambda = a \cdot Re^b$; 传热因子

$j = (\alpha / \rho u c_p) Pr^{2/3}$; 摩擦系数 $f = (P_2 - P_1) / (4l / d_e) \cdot (\rho u^2 / 2) = c \cdot Re^d$; p_2, p_1 —出口压力与入口压力, Pa; 对于空气 $Pr = 0.7$; $\rho = 1.225 \text{ kg/m}^3$; $\mu = 1.789 4 \times 10^{-5} \text{ Pa} \cdot \text{s}$; $\lambda = 0.024 2 \text{ W/(m}^2 \cdot \text{K)}$; $c_p = 1 006.43 \text{ J/(kg} \cdot \text{K)}$ 。

表 2 标准 $k-\epsilon$ 模型参数

c_{μ}	$c_{1\epsilon}$	$c_{2\epsilon}$	c_k	c_{ϵ}	c_f
0.09	1.44	1.92	1.0	1.3	0.9~1.0

2.3 边界条件与工况

边界条件: 定义波纹板表面为定壁温条件, $T = 323 \text{ K}$; 流体入口为速度入口, 本研究通过改变入口流速对空气在波纹倾角 $\beta = 30^\circ, 45^\circ$ 和 60° 的波纹流道内的流阻与传热状态进行模拟; 流体出口为压力出口; 其余表面为绝热边界条件。

工况: 流体入口的温度与速度均为均匀分布, 入口空气的温度为 $T = 253 \text{ K}$; 空气的定性温度是在进出口平均温度下定义。

2.4 控制方程的求解与验证

采用 SIMPLEST 算法求解控制方程, 偏微分方程的离散采取混合差分格式, 近壁面区采用壁面函数的处理方法。

Fluent 作为流体力学计算商业软件, 对于模拟复杂流场结构的不可压缩/可压缩流动来说具有理想的求解效果^[11~12]。通过实验对模拟的结果做了进一步验证, 图 5 为实验系统的设备原理图, 实验系统还包括有数据采集与处理系统。实验时采用与模拟相同的参数条件, 进口风速分别取 1, 2...8 m/s。由于板片模具的限制仅对波纹倾角 $\beta = 45^\circ$ 的板片进行了实验对比, 经整理后的 f 与 Nu 的值见图 7 和图 8。由图可见 f 的实验值大于模拟的结果, 相差的范围为 3%~15%; Nu 的值当空气流速低时略小于模拟值, 当空气流速高时又略大于模拟值, 相差的范围为 -9%~18%。模拟值与实验值虽然具有一定的偏差, 但从图中可以看出模拟值与实验值具有相近似的趋势, 模拟的结果可在一定程度上反映空气在波纹流道内的流动与传热的趋势并对工程应用具有借鉴意义。

3 计算结果和数据分析

图 6 显示了空气在流道内的流动状况, 流入流道的空气由于波纹倾角的阻挡, 可分解出一个与流

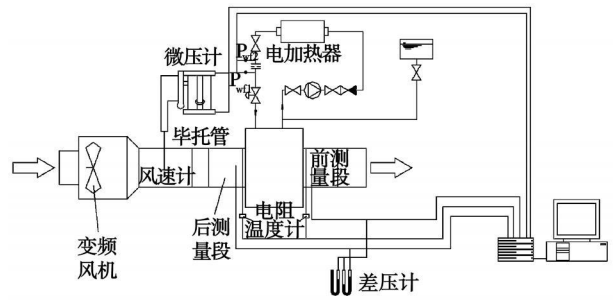


图 5 实验系统设备原理图

体流动方向垂直的切向力, 产生二次流, 导致空气在波纹板的凹凸波槽内做旋转运动, 形成二次涡旋, 强化对板片的冲刷, 破坏与减薄边界层, 从而实现了流体在板片间的传热强化。当波纹倾角较大时这种阻挡与掺混的作用最强, 但阻力损失也较大。



图 6 流道内空气的流动状况

3.1 计算区域空气流道的表面摩擦系数 f 的计算

表面摩擦系数反映的是波纹流道沿程与形状阻力对压降的影响, 一般随雷诺数的增大而减小。对模拟结果在不同流速下采用最小二乘法进行线性回归得到:

$$\begin{aligned} f &= 0.779 7 Re^{-0.390 9} & \beta &= 30^\circ \\ f &= 0.824 6 Re^{-0.263 5} & \beta &= 45^\circ \\ f &= 1.719 7 Re^{-0.211 6} & \beta &= 60^\circ \end{aligned}$$

如图 6 所示, 在相同截面(入口水力直径)条件下, 波纹倾角越大, 摩擦系数越大, 阻力消耗越大。随着波纹倾角的减小, 摩擦系数减小。

3.2 计算区域空气流道的努塞尔数 Nu 的计算

无量纲的努塞尔数 $Nu = \alpha d_e / \lambda$ 反映的是波纹板流道的对流换热与一定水力直径条件下的流体表层导热之比, 回归后得:

$$\begin{aligned} Nu &= 0.042 Re^{0.867 9}, & \beta &= 30^\circ \\ Nu &= 0.110 1 Re^{0.773 6}, & \beta &= 45^\circ \\ Nu &= 0.167 5 Re^{0.741}, & \beta &= 60^\circ \end{aligned}$$

在相同的雷诺数与水力直径条件下, 增大波纹倾角, 使流体的扰动增强, 破坏了边界层, 有利于强

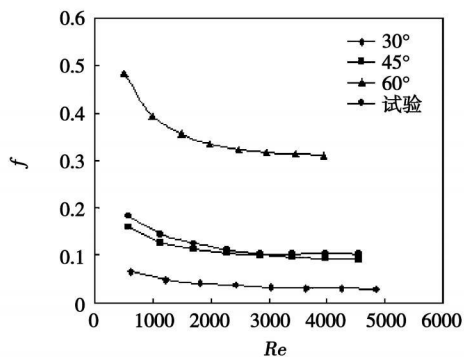


图 7 不同波纹倾角的 f

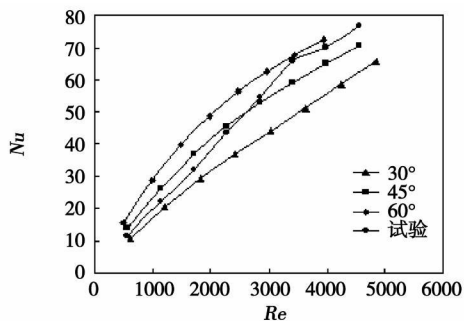


图 8 不同波纹倾角的 Nu

化传热过程,经计算在空气流速 5 m/s 时,波纹倾角 $\beta=45^\circ$ 时,板片表面具有较高的平均传热系数 $\alpha=154.54 \text{ W}/(\text{m}^2 \cdot \text{K})$ 。

3.3 计算区域空气流道的传热因子 j 与摩擦因子 f 的计算

传热因子 $j = (\alpha / \rho u c_p) Pr^{2/3}$ 实际表示的是一个无量纲的换热系数,它与摩擦系数 f 的比 j/f 表示在单位代价下的换热能力,即换热的效率。如图 9 所示,波纹倾角较小时 $\beta=30^\circ$ 换热效率最好。也就是说,在增加波纹倾角,获取较大的换热系数的同时,其阻力消耗也要增大。

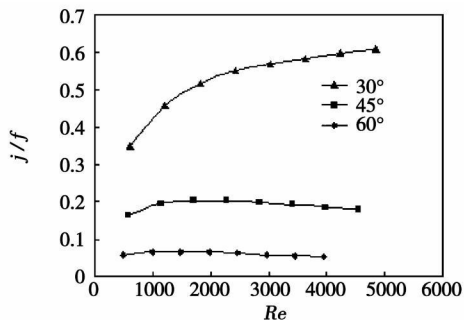


图 9 不同波纹倾角的 j/f

4 结 论

通过选取具有空气—水板式换热器典型结构的某一传热单元,可以用 Fluent 软件进行数值模拟。其结果虽与实验具有一定误差,但由于其趋势较为近似,可满足做进一步理论研究的需要。

波纹倾角对在其流道内流体的流动与传热过程具有较大的影响。在一定的流速下,波纹倾角的增大,强化了传热过程,提高了换热性能,但阻力消耗也随之增大。

增大波纹倾角可增加换热量,并没有提高换热的效率。但波纹倾角不是决定空气在波纹板间流阻与传热过程的唯一因素,还需进一步研究其它因素对这一过程的影响,如波纹高度、形状等,以期达到优化设计的目的,而数值模拟是实现这一过程的有效方法。

参考文献:

- [1] 李剑川. 空调运行管理手册—原理、结构、安装、维修[M]. 上海: 上海交通大学出版社, 2000.
- [2] 马虎根. 紧凑型回热器器面换热与阻力特性研究[J]. 上海理工大学学报, 2004, 26(5): 393—398.
- [3] 程宝华, 李先瑞. 板式换热器及换热装置技术应用手册[M]. 北京: 国防工业出版社, 2005.
- [4] 杨崇麟. 板式换热器工程设计手册[M]. 北京: 机械工业出版社, 1995.
- [5] FOCKE W W, ZACHARIADES J OLIVIER I. The effect of the corrugation Inclination angle on the thermohydraulic performance of plate heat exchangers[J]. Int. J. Heat and Mass Transfer, 1985, 28(8): 1469—1479.
- [6] ARUN HULEY, RAJM MANGLIK. Enhanced heat transfer characteristics of single-phase flows in a plate heat exchangers with mixed chevron plates[J]. Enhanced Heat Transfer, 1997, 4: 187—201.
- [7] BENT SUNDEN. Enhancement of convective heat transfer in rib-rooughened rectangular ducts[J]. Enhanced Heat Transfer, 1999, 6: 89—103.
- [8] 丁铁新, 曲伟, 高珊. 回热器空气流道单层波纹板流场的数值模拟和优化 // 第三届工程计算流体力学会议论文集[C]. 哈尔滨: 哈尔滨工业大学出版社, 2006: 218—223.
- [9] 阴继翔. 波纹通道板间距对通道内流动与换热的数值研究[J]. 热科学与技术, 2005, 4(2): 123—125.
- [10] 陶文铨. 数值传热学[M]. 西安: 西安交通大学出版社, 2002.
- [11] 高珊, 曲伟. CW 原表面回热器的芯体内流动与传热数值模拟[J]. 工程热物理学报, 2006, 27(3): 490—492.
- [12] 张冬洁. 微型燃气轮机回热器燃气腔结构优化[J]. 热能动力工程, 2006, 21(1): 10—13.

(编辑 韩锋)

nation with two kinds of boundary-condition treatment methods, a study has been conducted respectively of the flow and heat transfer performance of two types of longitudinally and internally finned tubes. During the study, a realizable $k-\epsilon$ two equation model was used for the turbulent flow calculation. The numerical simulation results obtained from the two calculation models were compared with test results. It has been found that the simulation results obtained from the turbulent flow model are closer to the test values than those obtained from the laminar flow model. In the meanwhile, it has also been found that the critical Reynolds Number for the flow in both internally finned tubes when developing from a laminar flow to a turbulent one is far less than that for the traditional bare tube. In the light of the simulation results obtained from the turbulent flow model, correlation formulae were obtained through a fitting for the two types of internally finned tubes of $Nu-Re$ and $f-Re$ respectively, thus extending the applicable scope of the test data. Through a field synergy principle, a contrast analysis of intensified heat exchange mechanism for both types of internally-finned tubes was quantitatively conducted. The results of the study show that the field synergy degree of longitudinally-ridged and internally-finned tubes is better than that of longitudinally flat-finned tubes, thereby playing a role of intensified heat transfer. **Key words:** internally-finned tube, forced convection, heat transfer characteristics, numerical simulation

波纹倾角 β 对空气在波纹流道内的流阻与传热影响的数值分析 = Numerical Analysis of the Influence of Corrugation Inclination Angle β on the Air Flow Resistance and Heat Transfer in Corrugated Flow Passages [刊, 汉] / WU Hua-xin, SUN Gang (College of Architectural Engineering, Harbin Engineering University, Harbin, China, Post Code: 150001), ZHOU Song (College of Power Engineering, Harbin Engineering University, Harbin, China, Post Code: 150001), TIAN Bao-ren (Jitai Heat Exchanges Manufacturing Factory, Siping, China, Post Code: 136001) // Journal of Engineering for Thermal Energy & Power. — 2008, 23(5). — 531 ~ 534

An air-water corrugated plate type heater differs from a traditional ribbed tube type heater. The former is a primary surface type heat exchanger and the surface of which in contact with a heat transfer medium directly takes part in a heat transfer process, featuring a compact structure and high efficiency. It can be used in such cases as air-water heating and heat energy recovery systems etc. to serve as hot wind curtains and air conditioner heaters etc. The authors have simulated the air flow resistance and heat transfer characteristics in flow passages at various corrugation inclination angles of $\beta = 30^\circ, 45^\circ, 60^\circ$ by utilizing CFD (Computational Fluid Dynamics) software Fluent, and calculated the surface friction coefficient f , Nusselt Number Nu and the ratio of heat transfer factor and surface friction coefficient j/f . The results of the study show that the corrugation inclination angle is an important factor influencing the flow resistance and heat transfer process of air in corrugated flow passages. Through relevant comparisons, the above research findings can provide definite guidelines for the further optimized design of air-water corrugation plate type heaters. **Key words:** air-water corrugated plate type heater, flow resistance, heat transfer, numerical characteristic analysis

高转速强漩流离心法聚氧聚氮装置研究 = Exploratory Study of a High Rotating Speed and Strong-whirlpool Centrifugal Method-based Oxygen and Nitrogen Collecting Device [刊, 汉] / WANG Xi-kui, CHEN Zheng-ju, HONG Guang-huan, MENG Zhao-jun (Energy Collection Research Institute, Shenyang Institute of Engineering, Shenyang, China, Post Code: 110136), // Journal of Engineering for Thermal Energy & Power. — 2008, 23(5). — 535 ~ 538

To solve the difficult problem of oxygen and nitrogen separation from air, an innovative structure of “rotating casing type axial compressor” is proposed to replace the traditional “rotating hub type axial compressor”. The main difference of the two structures lies in the fact that the blades of a “rotating hub type compressor” are installed on the wheel hub and can only realize air compression, while those of a “rotating casing type compressor” are installed on the inside of an inner casing, rotating in an outer casing, thus effecting air separation. The authors have described the theories of oxygen and nitrogen centrifugal separation and the centrifugal pressure boosting of the rotating casing compressor. The merits, technical feasibility and application approach of air whirlpool separation were also expounded. A sketch of the centrifugal method-based test rig for oxygen and nitrogen collection was given, which can realize an integration of three devices, namely: an air compressor, an oxygen and nitrogen separator and a combustion whirlpool generator. The ultimate aim is to remarkably enhance energy source application efficiency, fully utilize resources as well as to save energy and protect the environment. **Key words:** oxygen and nitrogen collection, rotating casing type compressor, oxygen and nitrogen centrifugal separation, strong whirlpool separation, theoretical analysis, alternative version exploration